Advances in Concrete Construction, *Vol. 2, No. 4 (2014) 261-280*
DOI: http://dx.doi.org/10.12989/acc.2014.2.4.261

Seismic risk assessment of deficient reinforced concrete frames in near-fault regions

Vui Van Cao[a], Hamid Reza Ronagh[*], Hassan Baji[b]

School of Civil Engineering, The University of Queensland, St. Lucia, Australia

(Received March 9, 2013, Revised August 29, 2014, Accepted December 3, 2014)

Abstract. In many parts of the world, reinforced concrete (RC) buildings, designed and built in accordance with older codes, have suffered severe damage or even collapse as a result of recent near-fault earthquakes. This is particularly due to the deficiencies of most of the older (and even some of the recent) codes in dealing with near fault events. In this study, a tested three-storey frame designed for gravity loads only was selected to represent those deficient buildings. Nonlinear time history analyses were performed, followed by damage assessment procedures. The results were compared with experimental observation of the same frame showing a good match. Damage and fragility analyses of the frame subjected to 204 pulse-type motions were then performed using a selected damage model and inter-storey drifts. The results showed that the frame located in near-fault regions is extremely vulnerable to ground motions. The results also showed that the damage model better captures the damage distribution in the frame than inter-storey drifts. The first storey was identified as the most fragile and the inner columns of the first storey suffered most damage as indicated by the damage index. The findings would be helpful in the decision making process prior to the strengthening of buildings in near-fault regions.

Keywords: risk assessment; damage analysis; fragility analysis; reinforced concrete frame; near-fault earthquake

1. Introduction

Considerable losses of human lives and property have been observed in recent near-fault earthquakes such as Northridge 1994, Kobe 1995, Chi-Chi 1999, and Bam 2003. These unfortunate events have signalled the need to do more research on near-fault seismic events, the necessity for risk assessment of the existing buildings, and a revision of structural design methods for these regions. The reasons for the devastating consequences of near fault earthquakes seem to be not only due to the strong near-fault pulse-type ground motions themselves but also to the deficiencies of non-seismically designed buildings designed and built using older codes that did not consider the near-fault effects (and in some cases even the far-fault effects) adequately. The historical milestone of the former issue was possibly recognised in the earthquake events of 1966

*Corresponding author, Senior Lecturer, Ph.D E-mail: h.ronagh@uq.edu.au
[a]Ph.D student. E-mail: v.caovan@uq.edu.au
[b]Ph.D student. E-mail: h.baji@uq.edu.au

http://www.techno-press.org/?journal=acc&subpage=7 ISSN:2287-5301(Print)2287-531X(Online)

at Parkfield and 1971 at San Fernando in California (Mavroeidis and Papageorgiou, 2003). These events caused a strong surge in the volume of publications related to the effects of near-fault ground motions on structures (Kalkan and Kunnath 2006).

Several studies have been performed recently to assess the structural performance of RC structures subjected to near-fault motions (Alavi and Krawinkler 2004; Choi *et al*. 2010; Liao *et al*. 2001; Yüksel and Sürmeli 2010). However, studies of damage or fragility of structures located in near-fault regions are rarely found in the literature. In this study, damage and fragility analyses of a non-seismically designed reinforced concrete (RC) frame subjected to pulse-type motions in near-fault regions were performed. Two hundred and four pulse-type earthquake records were selected to represent possible ground motions for a near-fault region. A three-storey RC frame designed for gravity load representing existing non-seismically designed buildings, which was tested by Bracci (1992) and published by Bracci *et al*. (1995), was considered in this study. A nonlinear time history procedure was used for analysing the structures. The extent of the information available in Bracci (1992) and Bracci *et al*. (1995) makes it possible to conduct a thorough study of the behaviour numerically, allowing direct and meaningful comparisons of the numerical results with the experimental observations. Analyses of the frame subjected to the selected pulse-type motions were then performed. This was followed by damage analyses using the inter-storey drift as an indicator of the damage level in addition to the damage index proposed by Park and Ang (1985). The fragility curves of non-seismically designed RC buildings were established in terms of the Velocity Spectrum Intensity (VSI) of 204 real near-fault pulse-type motions corresponding to the states of light, moderate, severe damage, and collapse. These fragility curves, which are for non-seismically designed buildings in near-fault pulse-type regions, show the vulnerability of those buildings and the potential losses. These can be used to help with the decision making process prior to the strengthening of buildings in near-fault regions.

2. Near-fault pulse-type ground motions

Near-fault earthquakes and their effects on structures have attracted considerable research attention in the fields of Seismology and Structural Engineering. The special characteristics of near-fault earthquakes from an engineering point of view were first recognized by Bertero *et al* (1978). Near-fault ground motions differ greatly from those of far-fault ground motions (Choi *et al*. 2010; Kalkan and Kunnath, 2006). Generally, near-fault earthquakes are strong dynamic motions. They usually have high peak ground acceleration (Lu and Lin 2009), intense velocity (Galal and Naimi 2008; Hatzigeorgiou 2010; Lu and Lin 2009), and large displacements (fling-step) (Galal and Ghobarah 2006; Park *et al*. 2004).

Near-fault records are generally of a pulse-type (Baker 2007), and show long pulse-type periods (2s to 5s) (Galal and Naimi, 2008; Krishnan 2007; Mollaioli *et al*. 2006). Seismic events recorded in near-fault regions vary depending on the faulting mechanism, direction of propagation and the possible static deformations (fling-step effects) (Kalkan and Kunnath, 2006; Somerville and Graves 1993). They can be divided into fault-normal and fault-parallel components. The former often produces higher demands on structures than the latter (Alavi and Krawinkler 2001). Near-fault earthquakes transmit high energy to structures at the onset of the record (Choi *et al*. 2008; Liao *et al*. 2001), which causes the structures respond differently from their response when subjected to far-fault earthquakes. Near-fault seismic events impose very high demands on the structures, forcing them to absorb a large portion of the input energy in a few large displacement

cycles (Kalkan and Kunnath, 2006; Manfredi *et al*. 2003; Mollaioli *et al*. 2006; Shih *et al*. 2007).

The Pacific Earthquake Engineering Research Center database software (PEER 2011) was used to select near-fault pulse-type motions. Two hundred and four available pulse-type records of 102 stations in different earthquakes occurring all over the world were selected. These are shown in Appendix A numbered from 001 to 102 with different Next Generation Attenuation numbers (NGA#).

The actual VSI of every record was determined using the SeismoSignal software ("SeismoSignal" 2010). The range of VSI varies from 42(cm) to 580(cm).

3. Selection of damage indicators

Inter-storey drift is one of the most common measures of structural response. It can be used to define the extent of damage in a structure. Table 1 shows the guidelines available in FEMA 356 (ASCE, 2000) for different damage levels.

In addition to drift, the Park and Ang (1985) damage model was selected for fragility analysis. It is shown in Eq. (1) as a combination of deformation and hysteretic energy due to an earthquake. This damage model is quite well known and has been widely used in many studies including those by Kim *et al*. (2005), Yüksel and Sürmeli (2010), Ghosh *et al*. (2011) and Bassam *et al*. (2011). The inclusion of the effect of cyclic loads and its clear classification of damage levels shown in Table 2 seem to be the reasons for the widespread use of the model. The legends shown in the first column are used to illustrate its corresponding damage levels and later used to express the damage of the frame presented in Sections 5 and 6. Park and Ang (1985) defined the damage index DI as

$$DI = \frac{u_m}{u_u} + \beta \frac{E_h}{F_y u_u} \tag{1}$$

Table 1 Damage levels in FEMA 356 (ASCE, 2000)

Damage level	Drift
Very light	No permanent drift is observed
Light	Transient drift < 1% and no or negligible permanent drift
Moderate	Transient drift < 2% and permanent drift < 1%
Severe	Transient or permanent drift < 4%

Table 2 Park and Ang (1985) damage classification

Legend	Damage index	Description
.	DI < 0.1	No damage or localized minor cracking
+	0.1 ≤ DI < 0.25	Minor damage: light cracking throughout
x	0.25 ≤ DI < 0.40	Moderate damage: severe cracking, localized spalling
▲	0.4 ≤ DI < 1 (0.8)	Severe damage: concrete crushing, reinforcement exposed
●	DI ≥ 1 (0.8)	Collapse

where, u_m is the maximum displacement of a single-degree-of-freedom (SDOF) system subjected to earthquake, u_u is the ultimate displacement under monotonic loading, E_h is the hysteretic energy dissipated by the SDOF system, F_y is the yield force and β is a parameter to include the effect of repeated loading. The value of β varies from 0.05-0.15 (Prakash and Belarbi 2010). The average value of β = 0.1, which was used by Yüksel and Sürmeli (2010), is employed in the study. DI $\geq$ 0.8 has been suggested to represent collapse (Tabeshpour *et al*., 2004). Park and Ang (1985) employed a weighting factor based on hysteretic energy (E_i) in order to compute the damage index for different storeys and for the overall structure.

It is worth mentioning that the Park and Ang (1985) damage model results in a positive damage index with any small elastic deformation as can be seen from the first part of the Eq. (1). This is a limitation of the model (Cao *et al*., 2014; 2011). However, this limitation, together with no specific upper limit (Cao *et al*. 2014; 2011), would be helpful for a fragility analysis.

4. Description of the case study frame

The model of a one-third scale three-storey RC frame designed only for gravity load is shown in Fig. 1. This scaled model was tested by Bracci (1992). Fig. 2 presents its dimensions (in inches) and reinforcement details. The average elastic modulus E_c of concrete was 24200 MPa and the average strength f_c' was 27.2 MPa (varying from 20.2 to 34.2 MPa). Table 3 shows four types of reinforcement and their properties.

The total weight of each floor was found to be approximately 120 kN, including the self-weight of beams, columns, slabs and additional weights attached to the model as can be seen in Fig. 1. Further details of the model can be found in Bracci (1992) and Bracci *et al*. (1995). The N21E ground acceleration component of the Taft earthquake, which occurred on 21 July 1952 at the

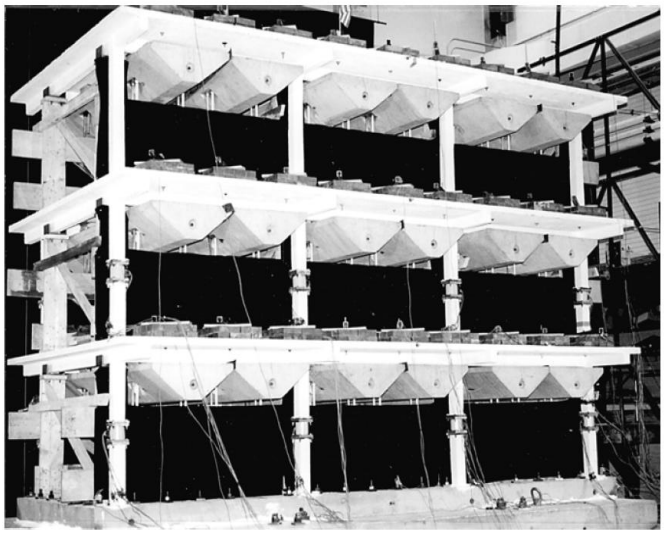

Fig. 1 Model of three storey frame (Bracci *et al*. 1995)

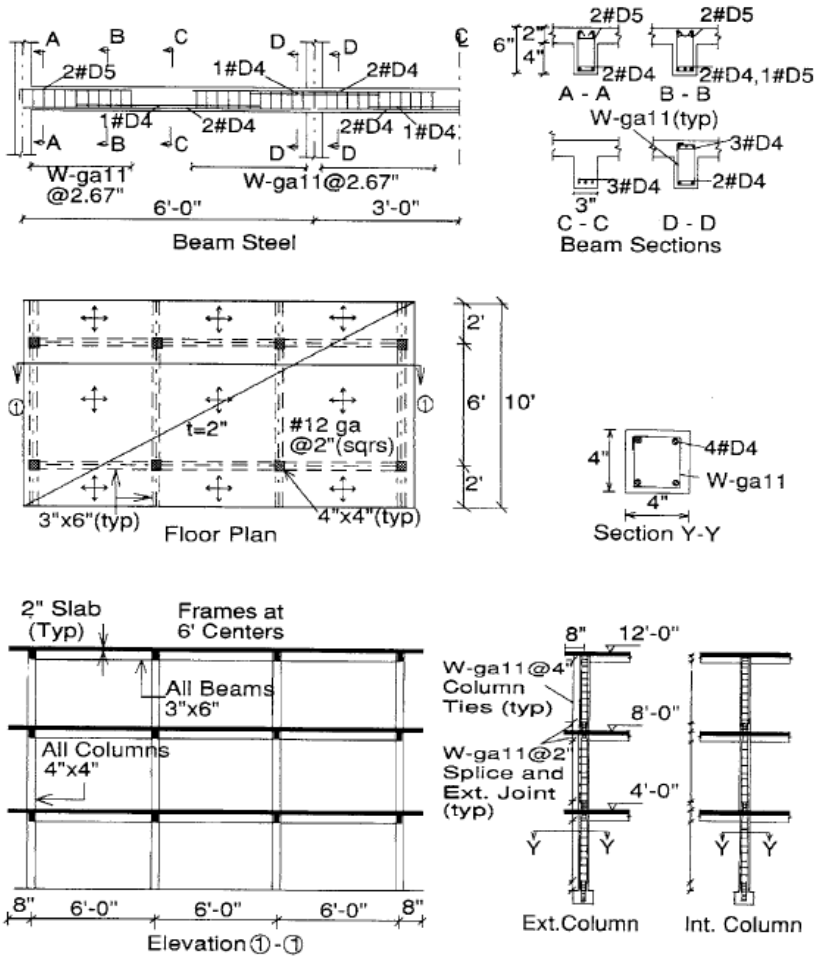

Fig. 2 Dimensions and reinforcement arrangement of three storey frame model (Bracci *et al*. 1995)

Table 3 Properties of reinforcement

Reinforcement	Diameter (mm)	Yield strength (MPa)	Ultimate strength (MPa)	Young Modulus (MPa)	Ultimate strain
D4	5.715	468.86	503.34	214089.8	0.15
D5	6.401	262.01	372.33	214089.8	0.15
12 ga.	2.770	399.91	441.28	206160.5	0.13
11 ga.	3.048	386.12	482.65	205471	0.13

Lincoln School Tunnel site in California, was used for the experiment. Minor, moderate and severe shakings were represented by different peak ground accelerations (PGA) of 0.05g, 0.20g and 0.30g, respectively.

5. Modelling and calibration

Some hysteretic models for RC members available in the literature include the cracking of concrete in the tension zone while some do not. In other words, some models are developed based on tri-linear curves whilst the rest are based on bi-linear curves. This characteristic can be used to classify those models into two types: tri-linear and bi-linear hysteretic models. The Takeda model (Takeda *et al*. 1970) is selected for use in this paper because it can represent the damage to an RC structure when the tension zone of concrete is cracked as shown in Fig. 3a, in which the coordinates (D_{cr}, P_{cr}) and (D_y, P_y) represent the cracking and yielding points respectively. Seven rules were developed to capture the response of the strutures subjected to cyclic loads as shown in Figs. 3b and 3c. The detailed descriptions of these rules can be found in Takeda *et al*. (1970).

The moment-curvature curves of reinforced concrete sections up to their ultimate are obtained using a fibre model, in which the cross section is discretised into many fibres. The strain distribution is assumed to be linear and the stress on each fibre is based on the material model with the strain defined at the centroid of that fibre. Behaviour of concrete is assumed to follow the modified the Kent and Park (1971) model made by Park *et al.* (1982) and simple model (Park and Paulay 1975) is used for steel. The iterated loops of strain distribution stop when the equilibrium conditions are achieved.

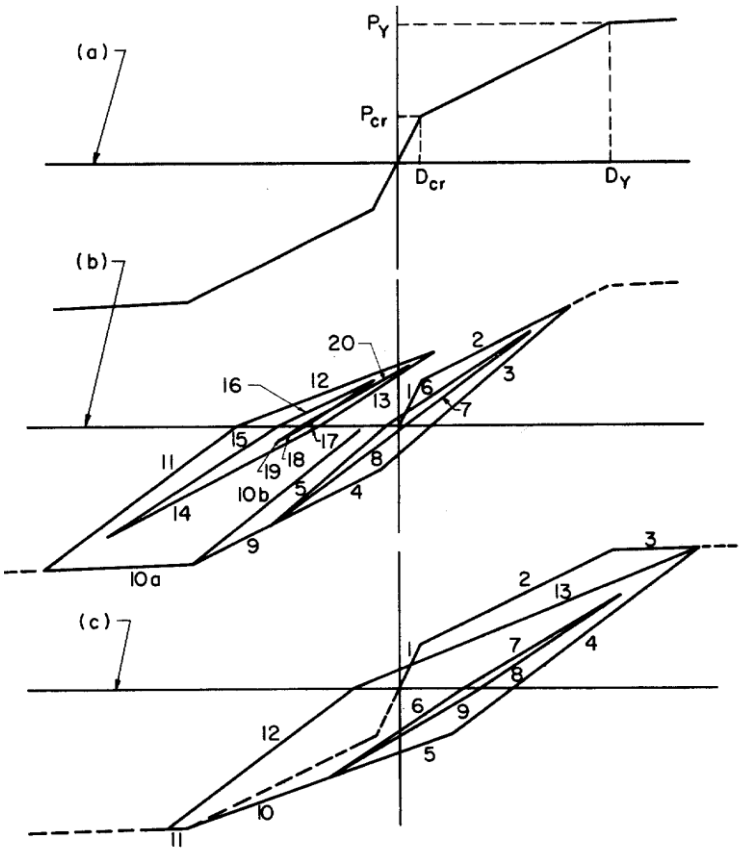

Fig. 3 Load-deflection relationship (Takeda *et al*. 1970)

The obtained moment-curvature curves are converted to moment-rotation curves, which are used for the nonlinear time history analyses, using the plastic hinge technique. The simple plastic hinge length $l_p = d$, where, d is the depth of the cross section, proposed by Sheikh and Khoury (1993) is adopted in this study. FEMA 356 (ASCE 2000) guidelines are followed to obtain the post-ultimate behaviour leading to collapse.

Table 4 shows the axial loads in columns which are assumed to be constant during earthquakes. The nonlinear Link element in SAP2000 is employed to model the structure as shown in Fig. 4. The SAP2000 nonlinear Link element allows for the incorporation of the moment-rotation property of the plastic hinge, and its behaviour follows the Takeda hysteretic model (Takeda *et al*., 1970) described above. Table 5 shows the first structural frequencies by comparison with those from the experiment. The first and second modes demonstrate a good match but there is little difference in the third mode. However, the first mode plays the most important role.

Table 6 presents the maximum inter-storey drifts and maximum storey displacements obtained from the model in comparison with those from the experiment (Bracci *et al*. 1995). Though not an exact match, an overall good approximation is demonstrated by the model.

Following the time history analyses, the selected Park and Ang (1985) damage model is employed to quantify the damage suffered by the frame during excitations. Figs. 5a, 6a and 7a show the experimental damage states obtained from (Bracci 1992) while Figs. 5b, 6b and 7b present the analytical damage states for the Taft PGAs of 0.05g, 0.20g and 0.30g, respectively. It is worth noting that different damage index levels of the analytical damage states are referred to the legends described in Table 2. The analytical damage states noticeably distinguish the damage for three shaking PGA intensities and are overall close to the experimental states. It should be noted that in the damage states obtained from analyses, DI < 0.1 in most of the positions in the frame is corresponding to "localized minor cracking" or "no damage". This is due to the limitations mentioned at the end of Section 3.

Table 4 Axial load in columns

Storey	Axial load (kN)	
	External column	Internal column
1	30	60
2	20	40
3	10	20

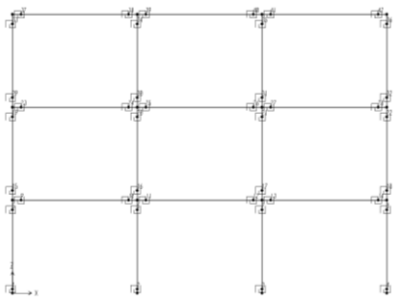

Fig. 4 Modelling of the three-storey frame with nonlinear Link elements

Table 5 Modal frequencies (Hz)

Mode	Experiment (Bracci *et al*. 1995)	Model
1	1.78	1.70
2	5.32	5.30
3	7.89	9.03

Table 6 Comparison between experimental (Bracci *et al*. 1995) and analytical results

PGA	Storey	Maximum inter-storey drift (%)		Maximum storey displacement (mm)	
		Experiment	Model	Experiment	Model
0.05g	3	0.23	0.21	7.6	7.9
	2	0.24	0.25	5.6	5.6
	1	0.28	0.23	3.6	2.8
0.20g	3	0.54	0.83	33.5	38.9
	2	1.07	1.17	29.0	30.7
	1	1.33	1.31	16.3	16.0
0.3g	3	0.89	1.18	59.7	58.4
	2	2.24	1.91	52.1	46.1
	1	2.03	1.96	24.6	23.9

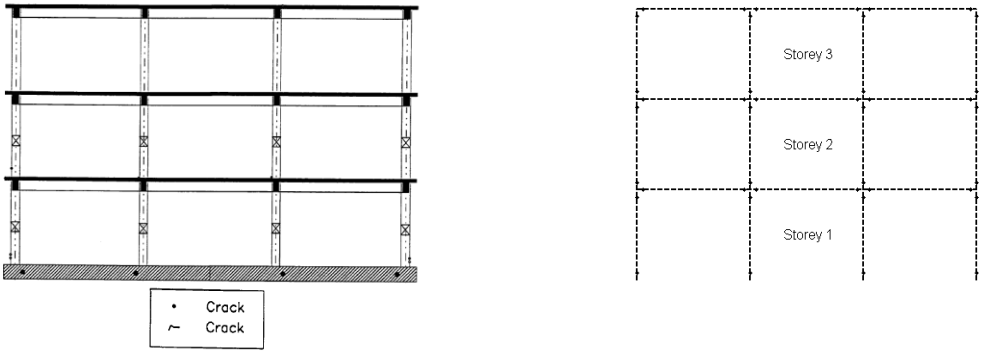

a) b)

Fig. 5 Damage states – Taft 0.05g: a) Experiment (Bracci 1992); b) Analysis

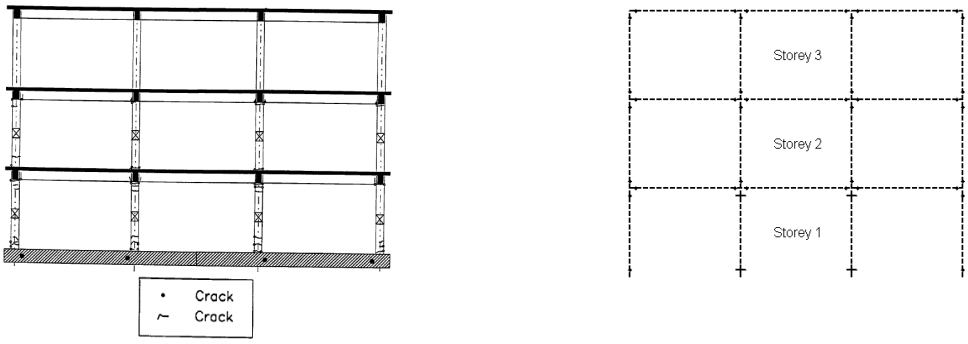

a) b)

Fig. 6 Damage states – Taft 0.30g: a) Experiment (Bracci 1992); b) Analysis

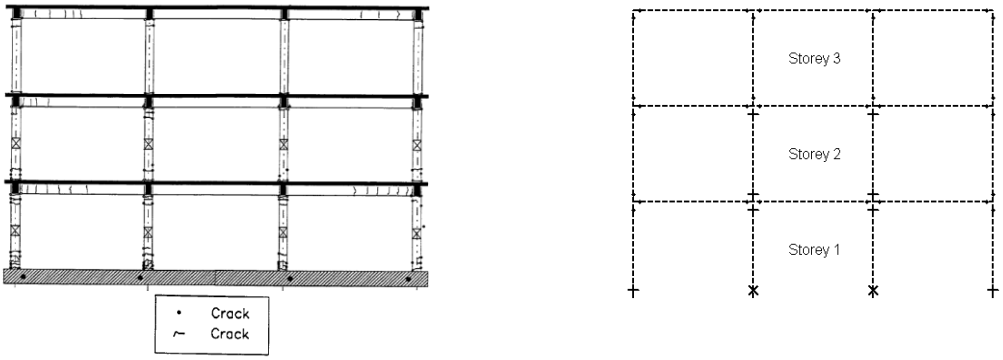

a) b)

Fig. 7 Damage states – Taft 0.30g: a) Experiment (Bracci 1992); b) Analysis

6. Time history, damage analyses and risk assessment

The structural model was subjected to the 204 selected pulse-type near-fault earthquake motions and the inter-storey drifts were identified. This was followed by damage analyses using the Park and Ang (1985) damage model. Fig. 8 shows the distribution of maximum inter-storey drift of each storey. It can be seen in Fig. 8 that the distribution of maximum inter-storey drifts of storeys 1 and 2 are similar while that of storey 3 shifts to a smaller inter-storey drift of 2%. Fig. 8 also shows that the probability of damage to storeys 1 and 2 is almost similar while being higher than that for storey 3. However, it fails to confirm that the first storey is the most fragile as was seen in the experiment.

Fig. 9 shows the average inter-storey drifts plotted in accordance with the potential damage levels based on FEMA 356 (ASCE 2000) guidelines. The average inter-storey drifts close to 4% show that the frame is on the verge of collapse. Fig. 9 also shows that storey 2 experiences the highest inter-storey drift, which misrepresents the damage patterns obtained from the experiment shown in Figs. 5a, 6a and 7a. This, together with the above distribution of maximum inter-storey drifts, shows that the inter-storey drift may not appropriately capture the distribution of damage in the frame.

Fig. 10 shows the average damage state, with the damage levels described in Table 2, of the frame subjected to 204 pulse-type motions. The first storey suffers the most damage while the third storey experiences the least. The most severe damage occurs in the two inner columns of the first storey. These locations are of importance for the whole structure as they can trigger the collapse of the whole building.

Fig. 11 shows the percentage of records which caused different levels of damage based on maximum inter-storey drifts. Only 4.4% of records caused light damage; 27.0% moderate while 33.3% and 35.3% caused severe damage and collapse, respectively. Overall, deficient buildings are extremely vulnerable to near-fault pulse-type motions as shown in Fig. 11 with a large percentage (68.6%) of the records causing severe damage and collapse.

Fragility is defined as the conditional probability of reaching or exceeding specified levels of damage under a given earthquake intensity which is represented by seismic parameters (Ellingwood, 2001). This concept is visually described by Park *et al.* (2009) as shown in Fig. 12. Fig. 12a describes the distribution of the structural response D for a given earthquake intensity S_{an}.

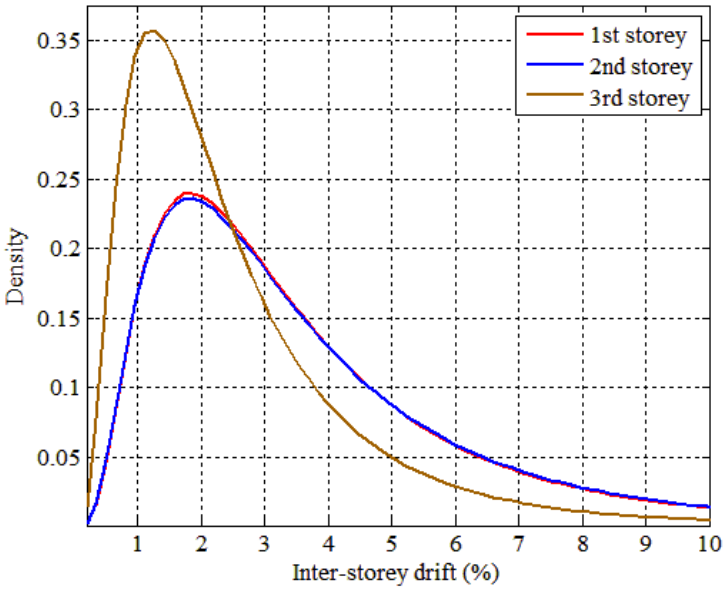

Fig. 8 Lognormal distribution of maximum inter-storey drifts

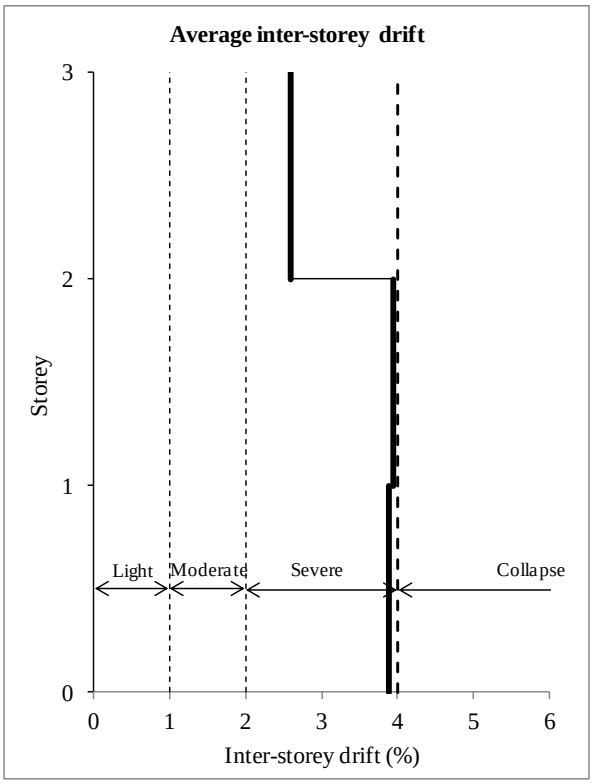

Fig. 9 Average inter-storey drifts vs damage states

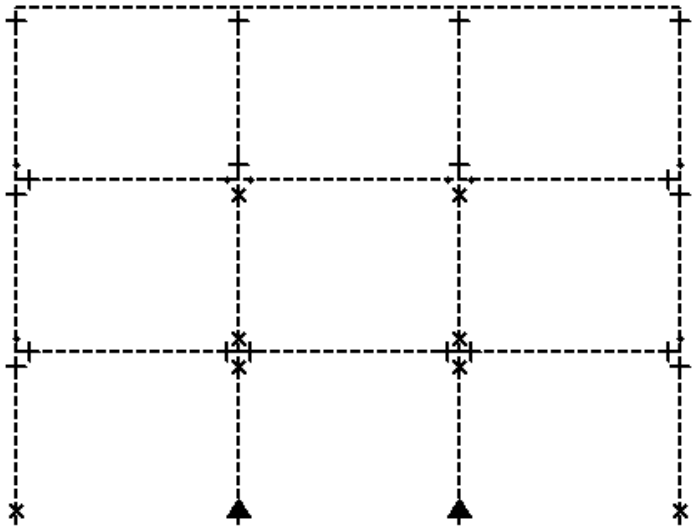

Fig. 10 Average damage state based on Park and Ang (1985) damage model

For each earthquake intensity, S_{an}, the probability of D exceeding the specified level of response, d_{si}, which can be written as $P[D \geq d_{si} \mid S_{an}]$ and called fragility, is determined as shown by the shaded area. Based on the fragility calculated, the fragility curve is constructed as shown in Fig. 12b. The fragility is mathematically shown in Eq. (2).

$$P(X \geq d_{si} \mid S_{an}) = \Phi\left(\frac{\ln X - \ln S}{\beta}\right) \tag{2}$$

where, Φ is the standard normal distribution, X is the lognormal distributed seismic parameters, S and β are the mean and the standard deviation of ln X.

A seismic parameter well representing the damage potential of structures should be selected as a hazard parameter. PGA is a commonly used seismic parameter; however, it demonstrates a weak correlation with the structural damage (Elenas 2000). In a study on correlation between seismic parameters and lining damage of mountain tunnels, Chen and Wei (2012) found that VSI correlates strongly with the lining damage. In a recent study on correlation between parameters of pulse-type motions and damage of low-rise RC frames, Cao and Ronagh (2014) found that VSI demonstrated the best correlation with the structural damage. Therefore, in this study, VSI is selected as the hazard parameter for constructing the fragility curves.

Figs 13 to 15 show the storey fragility curves for different damage states. Figs. 13a to 15a are established based on inter-storey drifts while Figs. 13b to 15b are based on the maximum Park and Ang damage index. It can be seen from the these figures that the fragility curves based on drifts of storey 1 and storey 2 are identical while the fragility curves based on the Park and Ang damage index are different for each storey. Based on the Park and Ang model, the first storey is the most fragile, followed by the second storey and then the third storey. These show that inter-storey drift can be a poor indicator of damage while the damage model of Park and Ang (1985) is clearly a better indicator. Figs. 13b to 15b show that the level of damage in the building is governed by the damage to storey 1, which is consistent with the experimental results.

Fig. 17 shows the fragility curves based on the maximum inter-storey drift and the maximum

damage index. The fragility curves based on Park and Ang damage index underestimate the damage of the frame in comparison with those based on inter-storey drift. As can be determined from Fig. 17b, the frame suffered moderate damage at the intensity of only approximately 125cm with probability of exceedance of 50%. In Figs. 17a and 17b, within the range of VSI from 42(cm) to 580(cm) of 204 near-fault pulse-type records, the fragility curves locate on the left corresponding to low levels of VSI.

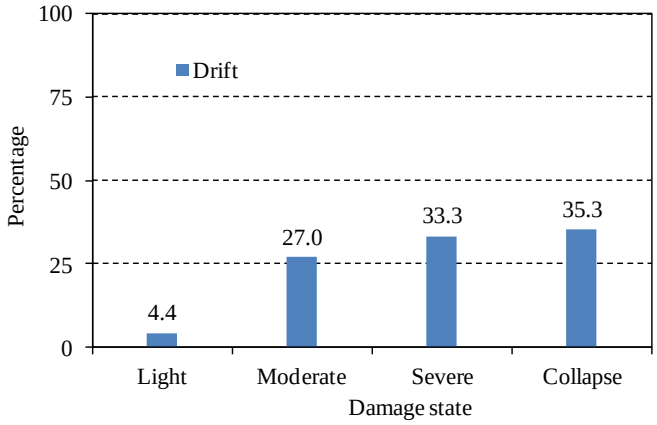

Fig. 11 Percentage for diffrent damage levels

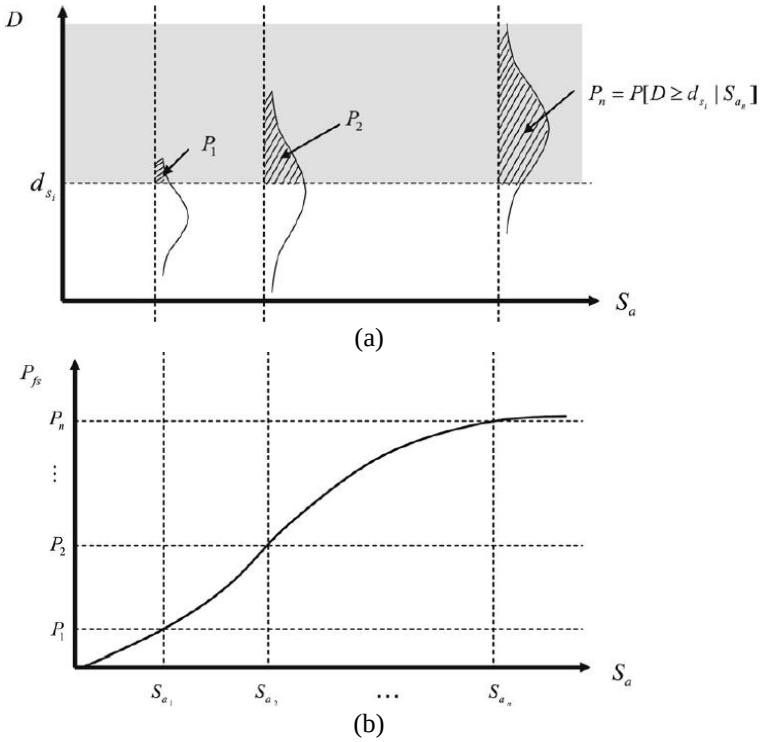

Fig. 12 Concept of fragility curve (Park *et al*. 2009)

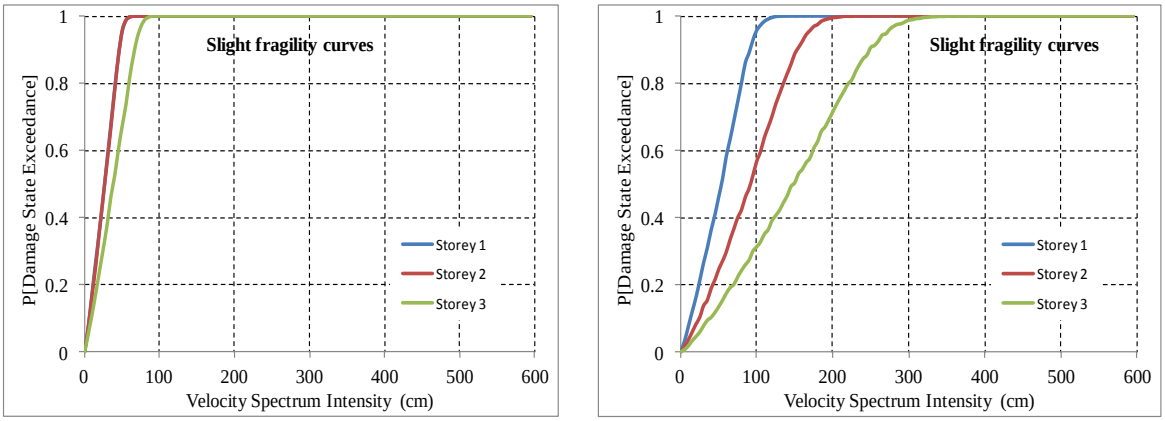

a) b)

Fig. 13 Storey fragility curves of slight damage based on: a) Drift; b) Park and Ang damage model

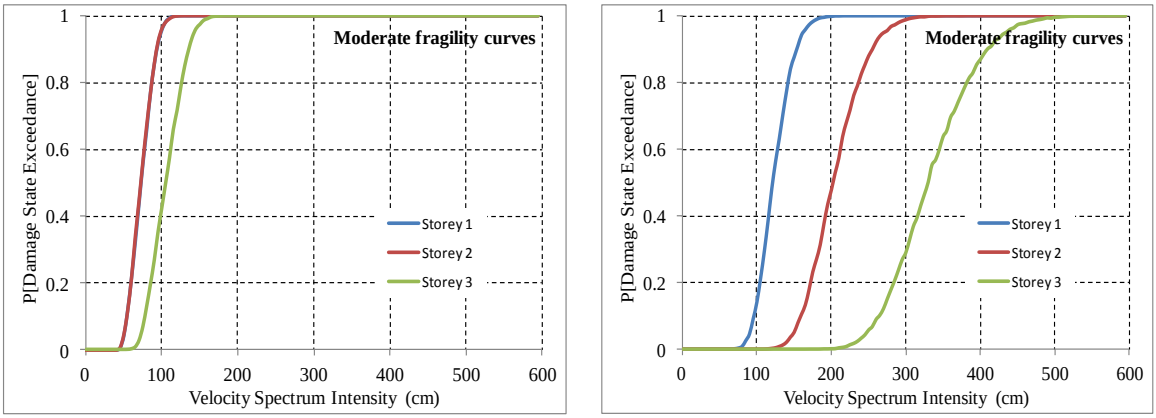

a) b)

Fig. 14 Storey fragility curves of moderate damage based on: a) Drift; b) Park and Ang damage model

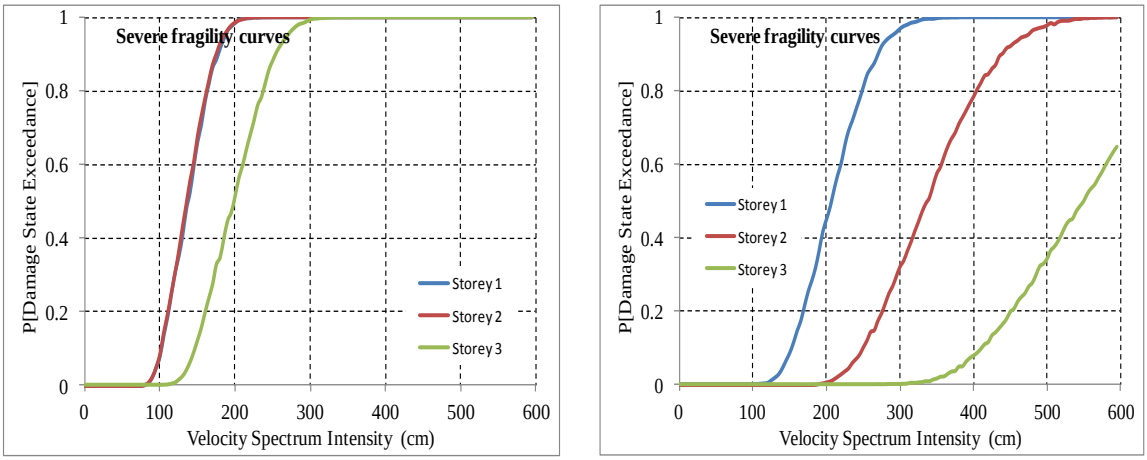

a) b)

Fig. 15 Storey fragility curves of severe damage based on: a) Drift; b) Park and Ang damage model

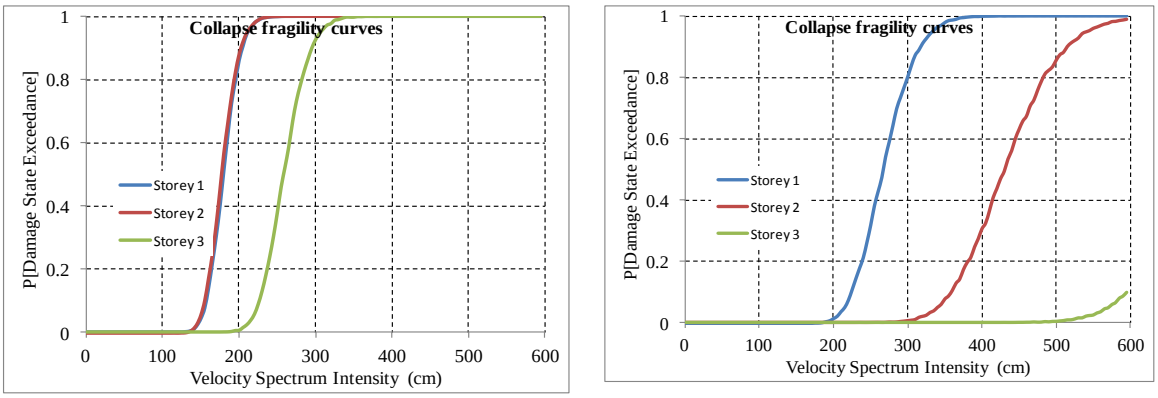

a) b)

Fig. 16 Fragility curves for different damage states based on: a) Maximum Drift; b) Maximum damage index

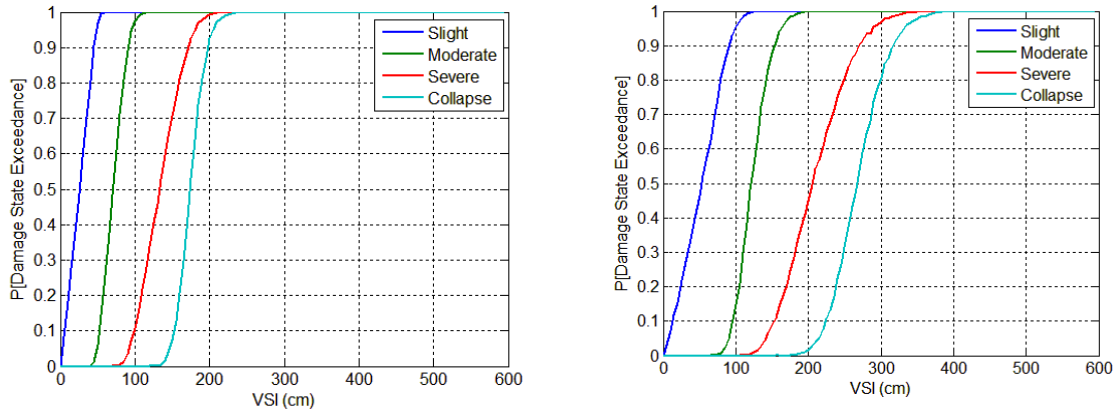

a) b)

Fig. 17 Fragility curves for different damage states based on: a) Maximum Drift; b) Maximum damage index

7. Conclusions

A previously tested non-seismically designed three-storey frame was modelled in SAP2000 using the nonlinear Link element with the Takeda model (Takeda *et al.* 1970). The analytical results obtained are consistent with those from the experiment for the N21E ground motion component of the Taft earthquake with three PGAs of 0.05g, 0.20g and 0.30g. Two hundred and four pulse-type records of worldwide near-fault earthquakes were selected to represent the possible ground motions in a near-fault region. The model was then subjected to these motions and damage and fragility analyses were performed based on the Park and Ang (1985) damage model and the commonly used parameter of inter-storey drift. The results show that the non-seismically designed RC frames were extremely vulnerable to near-fault pulse-type motions. The probability of severe damage and collapse was close to 70% when using inter-storey drift for the assessment of damage. Within the range of VSI from 42(cm) to 580(cm) of the selected near-fault motions, the frame suffered moderate damage at the intensity of only approximately 125cm with probability of exceedance of 50%. The results also revealed that inter-storey drift cannot be used to locate and

quantify the damage distributed in the frame and to appropriately capture the damage of different storeys; being so, it would not be a good damage indicator although it has been widely used. On the contrary, the Park and Ang (1985) damage model shows a better match to the experimental damage distributed at different locations.

Acknowledgements

The authors are grateful to Vietnam Ministry of Education and Training, and The University of Queensland for providing financial support towards this research. We also gratefully acknowledge the help provided by Jayadipta Ghosh from Department of Civil and Environmental Engineering, Rice University, US.

References

Alavi, B. and Krawinkler, H. (2001), Effects of near-fault ground motions on frame structures. Stanford: The John A. Blume Earthquake Engineering Center.

Alavi, B. and Krawinkler, H. (2004), "Behavior of moment-resisting frame structures subjected to near-fault ground motions", *Earthq. Eng. Struct. Dyn.*, **33**, 687-706.

ASCE (2000), Prestandard and commentary for the seismic rehabilitation of buildings, *Prepared for Federal Emergency Management Agency*, *FEMA Publication No. 356*. Washington, D.C.: Federal Emergency Management Agency.

Baker, J.W. (2007), "Quantitative classification of near-fault ground motions using wavelet analysis", *Bull. Seismol. Soc.Am.*, **97**(5), 1486-1501.

Bassam, A., Iranmanesh, A. and Ansari, F. (2011), "A simple quantitative approach for post earthquake damage assessment of flexure dominant reinforced concrete bridges", *Eng. Struct.*, **33**, 3218-3225.

Bertero, V.V., Mahin, S.A. and Herrera, R.A. (1978), "Aseismic design implications of near-fault San Fernando earthquake records", *Earthq. Eng. Struct. Dyn.*, **6**(1), 31-42.

Bracci, J.M. (1992), "Experimental and analytical study of seismic damage and retrofit of lightly reinforced concrete structures in low seismicity zones", Ph.D. Thesis, State University of New York at Buffalo.

Bracci, J.M., Reinhorn, A.M. and Mander, J.B. (1995), "Seismic resistance of reinforced concrete frame structures designed for gravity loads: performance of structural system", *ACI Struct. J.*, **92**(5), 597-608.

Cao, V.V. and Ronagh, H. (2014), "Correlation between parameters of pulse-type motions and damage of low-rise RC frames", *Earthq. Struct.*, **7(**3), 365-384, doi: http://dx.doi.org/10.12989/eas.2014.7.3.365

Cao, V.V., Ronagh, H., Ashraf, M. and Baji, H. (2011), "A new damage index for reinforced concrete structures subjected to seismic loads", *The First International Postgraduate Conference on Engineering, Designing and Developing the Built Environment for Sustainable Wellbeing -eddBE2011, The Queensland University of Technology, Queensland, Australia, 27-29 April 2011*, 194-199.

Chen, Z. and Wei, J. (2012), "Correlation between ground motion parameters and lining damage indices for mountain tunnels", *Natural Hazards*. doi: 10.1007/s11069-012-0437-5

Choi, H., Saiidi, M.S., Somerville, P. and El-Azazy, S. (2010), "Experimental study of reinforced concrete bridge columns subjected to near-fault ground motions", *ACI Struct. J.*, **107**(1), 3-12.

Choi, I.-K., Choun, Y.-S., Ahn, S.-M. and Seo, J.-M. (2008), "Probabilistic seismic risk analysis of CANDU containment structure for near-fault earthquakes", *Nuclear Eng. Des.*, **238**, 1382-1391.

Elenas, A. (2000), "Correlation between seismic acceleration parameters and overall structural damage indices of buildings", *Soil Dyn. Earthq. Eng.*, **20**, 93-100.

Ellingwood, B.R. (2001), "Earthquake risk assessment of building structures", *Reliab. Eng. Syst. Saf.*, **74**,

251-262.

Galal, K. and Ghobarah, A. (2006), "Effect of near-fault earthquakes on North American nuclear design spectra", *Nuclear Eng. Des.*, **236**, 1928-1936.

Galal, K. and Naimi, M. (2008), "Effect of soil conditions on the response of reinforced concrete tall structures to near fault earthquakes", *Struct. Des. Tall Spec. Build.*, **17**, 541-562.

Ghosh, S., Datta, D. and Katakdhond, A.A. (2011), "Estimation of the Park–Ang damage index for planar multi-storey frames using equivalent single-degree systems", *Eng. Struct.*, **33**, 2509-2524.

Hatzigeorgiou, G.D. (2010), "Behavior factors for nonlinear structures subjected to multiple near-fault earthquakes", *Comput. Struct.*, **88**, 309-321.

Kalkan, E. and Kunnath, S.K. (2006), "Effects of fling step and forward directivity on seismic response of buildings", *Earthq. spectra*, **22**(2), 367-390.

Kent, D.C. and Park, R. (1971), "Flexural members with confined concrete", *J. Struct. Div.*, **97**(7), 1969-1990

Kim, T.-H., Lee, K.-M., Chung, Y.-S. and Shinb, H.M. (2005), "Seismic damage assessment of reinforced concrete bridge columns", *Eng. Struct.*, **27**, 576-592.

Krishnan, S. (2007), "Case studies of damage to 19-storey irregular steel moment-frame buildings under near-source ground motion", *Earthq. Eng. Struct. Dyn.*, **36**, 861-885.

Liao, W.-I., Loh, C.-H. and Wan, S. (2001), "Earthquake responses of RC moment frames subjected to near-fault ground motions", *Struct. Des.Tall Spec.Buil.*, **10**, 219-29.

Lu, L.Y. and Lin, G.L. (2009), "Improvement of near-fault seismic isolation using a resettable variable stiffness damper", *Eng. Struct.*, **31**, 2097-2114.

Manfredi, G., Polese, M. and Cosenza, E. (2003), "Cumulative demand of the earthquake ground motions in the near source", *Earthq. Eng.Struct. Dyn.*, **32**, 1853-1865.

Mavroeidis, G. and Papageorgiou, A. (2003), "A mathematical representation of near-fault ground motions", *Bull. Seismol. Soc.Am.*, **93**(3), 1099-1131.

Mollaioli, F., Bruno, S., Decanini, L.D. and Panza, G.F. (2006), "Characterization of the dynamic response of structures to damaging pulse-type near-fault ground motions", *Meccanica*, **41**, 23-46.

Park, J., Towashiraporn, P., Craig, J.I. and Goodnod, B.J. (2009), "Seismic fragility analysis of low-rise unreinforced masonry structures", *Eng. Struct.*, **31**, 125-137.

Park, R. and Paulay, T. (Eds.), (1975), *Reinforced concrete structures*. New York - London - Sydney - Toronto: John Wiley & Sons.

Park, R., Priestley, M.J.N. and Gill, W.D. (1982), "Ductility of square-confined concrete columns", *J. Struct. Div.*, **108**, 929-950.

Park, S.W., Ghasemi, H., Shen, J. and Yashinsky, M. (2004), "Simulation of the seismic performance of the Bolu Viaduct subjected to near-fault ground motions", *Earthq. Eng. Struct. Dyn.*, **33**, 1249-1270.

Park, Y.-J. and Ang, A.H.-S. (1985), "Mechanistic seismic damage model for reinforced concrete", *J. Struct. Eng.*, **111**(4), 722-739.

PEER. (2011), PEER ground motion database. http://peer.berkeley.edu/peer_ground_motion_database.

Prakash, S.S. and Belarbi, A. (2010), "Towards damage-based design approach for RC bridge columns under combined loadings using damage index models", *J. Earthq. Eng.*, **14**(26), 363-389.

. SeismoSignal (Version 4.1.2). (2010). Pavia, Italy: Seismosoft Ltd. Retrieved from http://www.seismosoft.com/en/HomePage.aspx

Sheikh, S.A. and Khoury, S.S. (1993), "Confined concrete columns with stubs", *ACI Struct. J.*, **90**(4), 414-431.

Shih, M.H., Chen, C.L. and Sung, W.P. (2007), "Collapse analysis of building structures under excitation of near-fault ground motion with consideration of large deformation and displacement", *Struct. Des. Tall Spec. Build.*, **16**, 165-180.

Somerville, P. and Graves, R. (1993), "Conditions that give rise to unusually large long period ground mtions", *Struct. Des. Tall. Spec. Build.*, **2**, 311-232.

Tabeshpour, M.R., Bakhshi, A. and Golafshani, A.A. (2004), "Vulnerability and damage analyses of existing buildings", *13th World Conference on Earthquake Engineering*, Paper No. 1261.

Takeda, T., Sozen, M.A. and Nielsen, N.N. (1970), "Reinforced concrete response to simulated earthquakes", *J. Struct. Div.*, **96**, 2557-2573.

Yüksel, E. and Sürmeli, M. (2010), "Failure analysis of one-story precast structures for near-fault and far-fault strong ground motions", *Bull. Earthq. Eng.*, **8**, 937-953.

Appendix A Near fault pulse type motions

Name	NGA#	Event	Year	Station	Mag	Mechanism
001	150	Coyote Lake	1979	Gilroy Array #6	5.74	Strike-Slip
002	250	Mammoth Lakes-06	1980	Long Valley Dam (Upr L Abut)	5.94	Strike-Slip
003	316	Westmorland	1981	Parachute Test Site	5.9	Strike-Slip
004	319	Westmorland	1981	Westmorland Fire Sta	5.9	Strike-Slip
005	407	Coalinga-05	1983	Oil City	5.77	Reverse
006	415	Coalinga-05	1983	Transmitter Hill	5.77	Reverse
007	418	Coalinga-07	1983	Coalinga-14th & Elm (Old CHP)	5.21	Reverse
008	568	San Salvador	1986	Geotech Investig Center	5.8	Strike-Slip
009	569	San Salvador	1986	National Geografical Inst	5.8	Strike-Slip
010	615	Whittier Narrows-01	1987	Downey - Co Maint Bldg	5.99	Reverse-Oblique
011	645	Whittier Narrows-01	1987	LB - Orange Ave	5.99	Reverse-Oblique
012	158	Imperial Valley-06	1979	Aeropuerto Mexicali	6.53	Strike-Slip
013	159	Imperial Valley-06	1979	Agrarias	6.53	Strike-Slip
014	161	Imperial Valley-06	1979	Brawley Airport	6.53	Strike-Slip
015	170	Imperial Valley-06	1979	EC County Center FF	6.53	Strike-Slip
016	171	Imperial Valley-06	1979	EC Meloland Overpass FF	6.53	Strike-Slip
017	173	Imperial Valley-06	1979	El Centro Array #10	6.53	Strike-Slip
018	174	Imperial Valley-06	1979	El Centro Array #11	6.53	Strike-Slip
019	178	Imperial Valley-06	1979	El Centro Array #3	6.53	Strike-Slip
020	179	Imperial Valley-06	1979	El Centro Array #4	6.53	Strike-Slip
021	180	Imperial Valley-06	1979	El Centro Array #5	6.53	Strike-Slip
022	181	Imperial Valley-06	1979	El Centro Array #6	6.53	Strike-Slip
023	182	Imperial Valley-06	1979	El Centro Array #7	6.53	Strike-Slip
024	183	Imperial Valley-06	1979	El Centro Array #8	6.53	Strike-Slip
025	184	Imperial Valley-06	1979	El Centro Differential Array	6.53	Strike-Slip
026	185	Imperial Valley-06	1979	Holtville Post Office	6.53	Strike-Slip
027	451	Morgan Hill	1984	Coyote Lake Dam (SW Abut)	6.19	Strike-Slip
028	459	Morgan Hill	1984	Gilroy Array #6	6.19	Strike-Slip
029	529	N. Palm Springs	1986	North Palm Springs	6.06	Reverse-Oblique
030	721	Superstition Hills-02	1987	El Centro Imp. Co. Cent	6.54	Strike-Slip
031	722	Superstition Hills-02	1987	Kornbloom Road (temp)	6.54	Strike-Slip
032	723	Superstition Hills-02	1987	Parachute Test Site	6.54	Strike-Slip
033	2457	Chi-Chi, Taiwan-03	1999	CHY024	6.2	Reverse
034	2495	Chi-Chi, Taiwan-03	1999	CHY080	6.2	Reverse
035	2627	Chi-Chi, Taiwan-03	1999	TCU076	6.2	Reverse
036	3317	Chi-Chi, Taiwan-06	1999	CHY101	6.3	Reverse
037	3475	Chi-Chi, Taiwan-06	1999	TCU080	6.3	Reverse

Appendix A Continued

Name	NGA#	Event	Year	Station	Mag	Mechanism
038	77	San Fernando	1971	Pacoima Dam (upper left abut)	6.61	Reverse
039	292	Irpinia, Italy-01	1980	Sturno	6.9	Normal
040	496	Nahanni, Canada	1985	Site 2	6.76	Reverse
041	821	Erzican, Turkey	1992	Erzincan	6.69	Strike-Slip
042	983	Northridge-01	1994	Jensen Filter Plant Generator	6.69	Reverse
043	1009	Northridge-01	1994	LA - Wadsworth VA Hospital North	6.69	Reverse
044	1013	Northridge-01	1994	LA Dam	6.69	Reverse
045	1044	Northridge-01	1994	Newhall - Fire Sta	6.69	Reverse
046	1045	Northridge-01	1994	Newhall - W Pico Canyon Rd.	6.69	Reverse
047	1050	Northridge-01	1994	Pacoima Dam (downstr)	6.69	Reverse
048	1051	Northridge-01	1994	Pacoima Dam (upper left)	6.69	Reverse
049	1063	Northridge-01	1994	Rinaldi Receiving Sta	6.69	Reverse
050	1084	Northridge-01	1994	Sylmar - Converter Sta	6.69	Reverse
051	1085	Northridge-01	1994	Sylmar - Converter Sta East	6.69	Reverse
052	1086	Northridge-01	1994	Sylmar - Olive View Med FF	6.69	Reverse
053	1106	Kobe, Japan	1995	KJMA	6.9	Strike-Slip
054	1119	Kobe, Japan	1995	Takarazuka	6.9	Strike-Slip
055	1120	Kobe, Japan	1995	Takatori	6.9	Strike-Slip
056	738	Loma Prieta	1989	Alameda Naval Air Stn Hanger	6.93	Reverse-Oblique
057	763	Loma Prieta	1989	Gilroy - Gavilan Coll.	6.93	Reverse-Oblique
058	764	Loma Prieta	1989	Gilroy - Historic Bldg.	6.93	Reverse-Oblique
059	765	Loma Prieta	1989	Gilroy Array #1	6.93	Reverse-Oblique
060	766	Loma Prieta	1989	Gilroy Array #2	6.93	Reverse-Oblique
061	767	Loma Prieta	1989	Gilroy Array #3	6.93	Reverse-Oblique
062	779	Loma Prieta	1989	LGPC	6.93	Reverse-Oblique
063	784	Loma Prieta	1989	Oakland - Title & Trust	6.93	Reverse-Oblique
064	802	Loma Prieta	1989	Saratoga - Aloha Ave	6.93	Reverse-Oblique
065	803	Loma Prieta	1989	Saratoga - W Valley Coll.	6.93	Reverse-Oblique
066	825	Cape Mendocino	1992	Cape Mendocino	7.01	Reverse
067	828	Cape Mendocino	1992	Petrolia	7.01	Reverse
068	838	Landers	1992	Barstow	7.28	Strike-Slip
069	879	Landers	1992	Lucerne	7.28	Strike-Slip
070	900	Landers	1992	Yermo Fire Station	7.28	Strike-Slip
071	1602	Duzce, Turkey	1999	Bolu	7.14	Strike-Slip
072	1605	Duzce, Turkey	1999	Duzce	7.14	Strike-Slip
073	1148	Kocaeli, Turkey	1999	Arcelik	7.51	Strike-Slip
074	1176	Kocaeli, Turkey	1999	Yarimca	7.51	Strike-Slip

Appendix A Continued

Name	NGA#	Event	Year	Station	Mag	Mechanism
075	1182	Chi-Chi, Taiwan	1999	CHY006	7.62	Reverse-Oblique
076	1193	Chi-Chi, Taiwan	1999	CHY024	7.62	Reverse-Oblique
077	1202	Chi-Chi, Taiwan	1999	CHY035	7.62	Reverse-Oblique
078	1244	Chi-Chi, Taiwan	1999	CHY101	7.62	Reverse-Oblique
079	1410	Chi-Chi, Taiwan	1999	TAP003	7.62	Reverse-Oblique
080	1411	Chi-Chi, Taiwan	1999	TAP005	7.62	Reverse-Oblique
081	1463	Chi-Chi, Taiwan	1999	TCU003	7.62	Reverse-Oblique
082	1464	Chi-Chi, Taiwan	1999	TCU006	7.62	Reverse-Oblique
083	1468	Chi-Chi, Taiwan	1999	TCU010	7.62	Reverse-Oblique
084	1471	Chi-Chi, Taiwan	1999	TCU015	7.62	Reverse-Oblique
085	1473	Chi-Chi, Taiwan	1999	TCU018	7.62	Reverse-Oblique
086	1475	Chi-Chi, Taiwan	1999	TCU026	7.62	Reverse-Oblique
087	1476	Chi-Chi, Taiwan	1999	TCU029	7.62	Reverse-Oblique
088	1477	Chi-Chi, Taiwan	1999	TCU031	7.62	Reverse-Oblique
089	1479	Chi-Chi, Taiwan	1999	TCU034	7.62	Reverse-Oblique
090	1480	Chi-Chi, Taiwan	1999	TCU036	7.62	Reverse-Oblique
091	1481	Chi-Chi, Taiwan	1999	TCU038	7.62	Reverse-Oblique
092	1482	Chi-Chi, Taiwan	1999	TCU039	7.62	Reverse-Oblique
093	1483	Chi-Chi, Taiwan	1999	TCU040	7.62	Reverse-Oblique
094	1484	Chi-Chi, Taiwan	1999	TCU042	7.62	Reverse-Oblique
095	1486	Chi-Chi, Taiwan	1999	TCU046	7.62	Reverse-Oblique
096	1489	Chi-Chi, Taiwan	1999	TCU049	7.62	Reverse-Oblique
097	1492	Chi-Chi, Taiwan	1999	TCU052	7.62	Reverse-Oblique
098	1493	Chi-Chi, Taiwan	1999	TCU053	7.62	Reverse-Oblique
099	1494	Chi-Chi, Taiwan	1999	TCU054	7.62	Reverse-Oblique
100	1496	Chi-Chi, Taiwan	1999	TCU056	7.62	Reverse-Oblique
101	1498	Chi-Chi, Taiwan	1999	TCU059	7.62	Reverse-Oblique
102	1499	Chi-Chi, Taiwan	1999	TCU060	7.62	Reverse-Oblique